

Article

# Microreactor Based on Trimetallic Nano-Oxides Obtained by In Situ Growth from German Silver

Ana P. Cabello, Mayra A. Franco Murcia , María A. Ulla and Juan M. Zamaro \* 

Instituto de Investigaciones en Catálisis y Petroquímica, INCAPE (FIQ, UNL, CONICET),  
Santiago del Estero 2829, Santa Fe 3000, Argentina; apcabello@fiq.unl.edu.ar (A.P.C.);  
mafrancomurcia@fiq.unl.edu.ar (M.A.F.M.); mulla@fiq.unl.edu.ar (M.A.U.)

\* Correspondence: zamaro@fiq.unl.edu.ar; Tel.: +54-0342-4536861

**Abstract:** Nanostructured films of copper, zinc, and nickel oxides were obtained from a controlled oxidation of the ternary nickel silver (Cu-Zn-Ni) substrates through a one-pot, green, and low temperature vapor-based treatment. Brief contact of the alloy with ammonia and hydrogen peroxide vapors at room temperature originates a mixture of nanometric copper, zinc, and nickel oxides at its surface. The growths evolve with time and temperature, generating a layered film with highly dispersed copper nano-oxides/hydroxides on a base of zinc and nickel oxides. The composition, configuration, and way of obtaining these films make them green catalysts, which are highly active and stable for a carbon monoxide oxidation reaction.

**Keywords:** nickel brass; alpacca; copper; zinc; nickel; catalysis; CO oxidation



**Citation:** Cabello, A.P.; Franco Murcia, M.A.; Ulla, M.A.; Zamaro, J.M. Microreactor Based on Trimetallic Nano-Oxides Obtained by In Situ Growth from German Silver. *Catalysts* **2023**, *13*, 932. <https://doi.org/10.3390/catal13060932>

Academic Editors: Marcela Martínez Tejada and Miguel Ángel Centeno

Received: 28 April 2023

Revised: 20 May 2023

Accepted: 22 May 2023

Published: 25 May 2023



**Copyright:** © 2023 by the authors. Licensee MDPI, Basel, Switzerland. This article is an open access article distributed under the terms and conditions of the Creative Commons Attribution (CC BY) license (<https://creativecommons.org/licenses/by/4.0/>).

## 1. Introduction

One of the current challenges in catalysis is to develop catalysts free of noble metals since these elements are expensive and have a low natural abundance, which is why they are currently considered unsustainable options [1]. This has prompted a growing interest in the study of catalysts based on non-noble metal oxides given their higher availability, lower cost, and resistance to poisoning by sulfur compounds and water vapor compared to noble metals [2]. However, it should be considered that not only the active element is part of the concept of a green catalyst but also its configuration and the support material. Pursuing these precepts, microreactors based on nano-oxides have been investigated to be applied in oxidation reactions, such as the CO oxidation, which is a highly exothermic reaction with strong environmental-energy implications. On the one hand, it is of interest to remove carbon monoxide from the atmosphere given the high toxicity of this gas for human and animal life [3]. Carbon monoxide is a common contaminant of hydrogen streams that poisons platinum-based catalysts of PEMFC type fuel cells [4]. For the CO oxidation reaction, catalysts based on noble metals such as Au, Pt, and Pd have traditionally been used [5–7], although among them, the most widely used systems have been those based on supported gold such as Au/ZnO-ZrO<sub>2</sub>, Au/CeO<sub>2</sub>, or Au/Co<sub>3</sub>O<sub>4</sub>-CeO<sub>2</sub> [8–10]. However, as mentioned above, the search for noble metals-free catalysts in recent years has led to the development of systems based on mono- and multi-metallic oxides. These types of nanostructured oxides have shown an acceptable catalytic efficiency, for example CuO/ZnO nanorods, Cu/CeO<sub>2</sub> nanosheets, Co<sub>3</sub>O<sub>4</sub>/CuO-MnO<sub>2</sub> nanowires, CuO/CeO<sub>2</sub>/ZrO<sub>2</sub>, and La-Pt-CoO/Al<sub>2</sub>O<sub>3</sub> nanostructures, and also some of these systems that are shaped as films, including FeCuO<sub>x</sub> and FeO<sub>x</sub>/Pt/Al<sub>2</sub>O<sub>3</sub> [11–18]. Taylor et al. [19] synthesized catalysts by coprecipitation, making intimate mixtures of ZnO and CuO, which were very active in this reaction. Wang et al. [20], as well as Jeong et al. [21], found that catalysts based on NiO nanoparticles were also active and stable in the CO oxidation. Furthermore, Chen et al. [22] observed that ZrO<sub>2</sub>-supported CuO-NiO catalysts provided a high level of CO conversion at low temperatures. Similarly, El-Shobaky et al. [23] found that when the catalyst was

composed of an intimate mixture of ZnO and NiO, a synergistic catalytic effect developed. It should be noted that there is a vast literature regarding the effect of the operational variables of this reaction. Numerous investigations have been carried out applying various operating conditions, such as space velocity, type of reactor, and reactant concentration, among others, whose description is outside the scope of this work and can be found in recent reviews on catalysts for this reaction [24].

It is possible to obtain the above-mentioned types of oxides with nanometric dimensions and highly dispersed onto copper alloy substrates. These types of alloys are relatively low-cost materials, easily available in a wide range of configurations and have high thermal conductivity [25]. In particular, this latter aspect is of relevance for the development of green, efficient catalysts designed to be used in highly exothermic reactions [26]. Taking these criteria into account, CuO<sub>x</sub>-based nanostructured films, adherent and adjustable in terms of their composition and morphology, were synthesized from the oxidation of copper substrates [27]. When such films were placed in a microreactor, a remarkable catalytic performance and stability in the CO oxidation was observed [28]. Recently, nanostructured CuO<sub>x</sub>-ZnO growths have been obtained from the controlled oxidation of brass substrates, which provide efficient microreactors due to the intimate contact between both nanometric oxide phases [29]. In this scenario, the alloy commercially known as German silver is positioned as an interesting alternative that would make it possible to obtain multi-metallic nano-oxide films. German silver is a ternary alloy with a general composition of 60–65% Cu, 17–19% Ni, and 17–23% Zn, and it has ductility, machinability at room temperature as well as resistance to wear and corrosive media [30]. Recently, Amin et al. applied hydrothermal synthesis on this type of substrate using NaHCO<sub>3</sub> solutions (453 K, 18 h) to obtain Cu<sub>2</sub>ZnNiO<sub>3</sub> nanowires that were used as photoelectrodes for water splitting [31]. For this same photoelectrochemical application, Bahnasawy et al. [32] synthesized mixed Cu–Zn oxide nanoparticles by anodization of German silver followed by its annealing in air at high temperature.

Within the context described above, the present work aims to study the in-situ growth of Cu–Zn–Ni nano-oxide mixtures from the controlled oxidation of German silver substrates, through a simple oxidation method and under mild conditions. The reason behind this work is the development of catalysts free of noble metals, based on catalytic films of mixed nano-oxides in which synergy could be established between such phases in close contact, yielding efficient films for the CO oxidation reaction.

## 2. Results and Discussion

### 2.1. Physicochemical Characteristics of the Nano-Oxide Film

#### 2.1.1. Evolution of Growth with Time

After treatment at 80 °C, substrates showed a progressive mass increase with the extension of the treatment time, which corresponds to the mass of oxygen incorporated during the oxidation process. First, they increased linearly but over longer periods of time, they began to attenuate slightly both in flat and micro-channeled substrates (Figure 1a). This shows that the growth rate of the oxides gradually decreases due to a higher difficulty in the migration of metals from the interface and/or oxygen from the surface of the film being formed as its thickness increases. Moreover, a visual change due to the formation of oxide layers that became denser with the synthesis time was noted, with a progressive darkening of the substrate surface (Figure S1). In all samples, the diffraction lines of the substrate showed a marked intensity, indicating the development of thin oxide films. The integrated area of the most important XRD peak of the substrate ( $2\theta$  42.7°) for the different treatment times allowed revealing a decrease in its intensity, which correlates well with a progressive increase in the film thickness, also in line with the mass gain trend (Figure 1b).

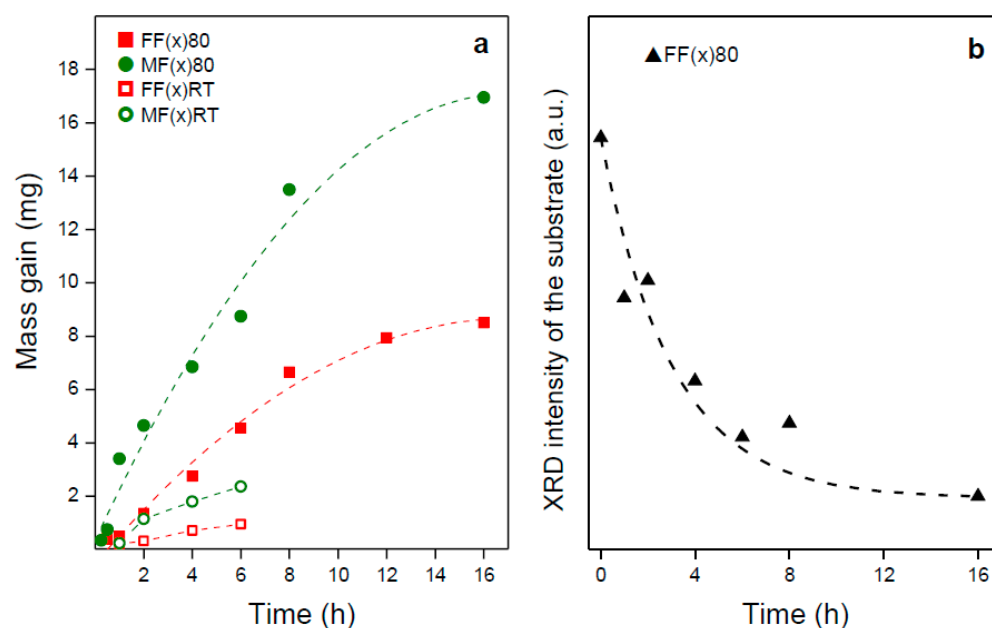


**Figure 1.** (a) Average mass gain of samples obtained after oxidation treatments (square: flat foils, circle: micro-folded foils, filled symbol: 80 °C, empty symbol: room temperature); (b) Integrated intensity of the main XRD peaks (42.7°) of foil substrates as a function of the synthesis time at 80 °C.

In all samples treated at this temperature (80 °C), it was possible to identify  $\text{Cu}(\text{OH})_2$ ,  $\text{CuO}$ ,  $\text{ZnO}$ , and  $\text{NiO}$  species (Figure 2). At short treatment times,  $\text{CuZnNi}(1)80$ , signals of the (020) and (021) planes from the orthorhombic  $\text{Cu}(\text{OH})_2$  structure (JCPDS 35-505), of the (111) planes from  $\text{CuO}$  (JCPDS 48-1548) and of the (002) planes from the hexagonal  $\text{ZnO}$  structure (JCPDS 36-1451), were distinguished. It should be noted that cupric hydroxide persisted at long treatment times, whereas  $\text{CuO}$  was detectable even at a short synthesis time. In the case of  $\text{ZnO}$ , an intensification of the (002) peak in comparison with the experimental pattern of the powder of this oxide was observed, indicating a preferred crystallographic orientation [33]. When analyzing case by case as the treatment time increased, it could be observed for the  $\text{CuZnNi}(2)80$  sample that, in addition to the above phases, there emerged the peak of the (11-1) plane from  $\text{CuO}$ , which intensified over time. For the  $\text{CuZnNi}(6)80$  sample, weak  $\text{NiO}$  signals began to be observed (JCPDS 47-1049). This evolution of the nano-oxide growth can be better appreciated in the zoom depicted in Figure 2b.

The bare and cleaned substrate showed a surface with some striations and irregularities that were present in this common commercial substrate, coming from its manufacturing process. The elemental EDS mapping corroborated a homogeneous spatial distribution of Cu, Zn, and Ni with an atomic composition of  $\text{Cu}:\text{Zn}:\text{Ni} = 66:20:14$  (Figure S2). The  $\text{Cu}/\text{Zn}$  atomic ratio was 3.2,  $\text{Cu}/\text{Ni}$  was 4.6, and  $\text{Zn}/\text{Ni}$  was 1.4 (Table 1). When this substrate was exposed to the treatment for one hour,  $\text{CuZnNi}(1)80$ , a change in the surface morphology was noted with a total coverage of small irregular growths (Figure 3a). Contrasting the elemental mapping (Figure 3a right) with the XRD, it follows that such growths correspond to  $\text{Cu}(\text{OH})_2$ ,  $\text{CuO}$ , and  $\text{ZnO}$  species, while the elemental atomic ratios (Table 1) suggest that the segregation of these oxides was not selective among them. Elemental mapping in other sectors of the same sample confirmed this effect (Figure S4). When the treatment was extended to two hours,  $\text{CuZnNi}(2)80$ , a surface could be seen covered by crystals in which two morphologies were distinguished (Figure 3b): regions with dense growths of prismatic crystals and some regions with small globular growths, whose morphological detail could be appreciated in observations at higher magnifications (Figure S3). According to the EDS analysis of this sample (Figure 3b right), the first corresponds to copper oxides/hydroxides while the second corresponds to zinc and nickel oxides, in line with

the increase in the proportion of both copper and zinc oxides compared to that of nickel (Table 1). As time progressed, CuZnNi(6)80, the copper oxide evolved to prismatic ( $\mu$ -PR) and globular-shaped ( $\mu$ -GL) micrometer-sized structures with size heterogeneity, as shown in Figure 3c. A stratification of the oxides was clearly defined with these copper-based species above an incipient growth of nanoflakes of zinc and nickel oxides, as observed in higher magnification images (Figure S5). These observations are in agreement with XRD results. The trend in the elemental atomic ratios of this sample (Table 1) agrees with a growth that began to be enriched in nickel oxide. Then, the films obtained at 80 °C allowed us to conclude that there was an evolution in the oxide growth onto German silver substrate, as the upper region of the film was enriched in copper species after up to six hours of treatment while the lower region was enriched in zinc and nickel species (Figure 3c right).

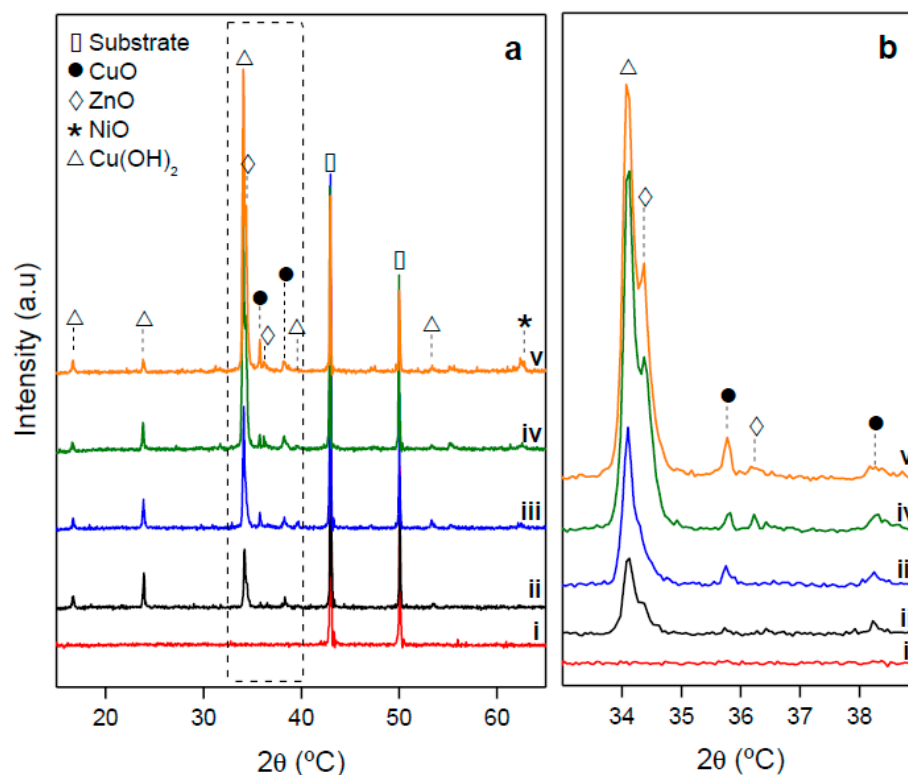


**Figure 2.** (a) XRD patterns of films grown on German silver substrates at 80 °C: (i) substrate; (ii) CuZnNi(1)80; (iii) CuZnNi(2)80; (iv) CuZnNi(4)80; (v) CuZnNi(6)80; (b) Detail of the diffractograms between  $2\theta$  33° and 39°.

**Table 1.** Elemental atomic composition obtained from EDS analyses of films synthesized at 80 °C and at room temperature.

Sample	Cu/Zn	Cu/Ni	Zn/Ni
Substrate	3.2	4.6	1.4
CuZnNi(1)80	3.2	4.3	1.4
CuZnNi(2)80	3.9	8.0	2.1
CuZnNi(6)80	3.4	4.1	1.2
CuZnNi(1)RT	3.2	4.8	1.5
CuZnNi(2)RT	4.6	6.1	1.3

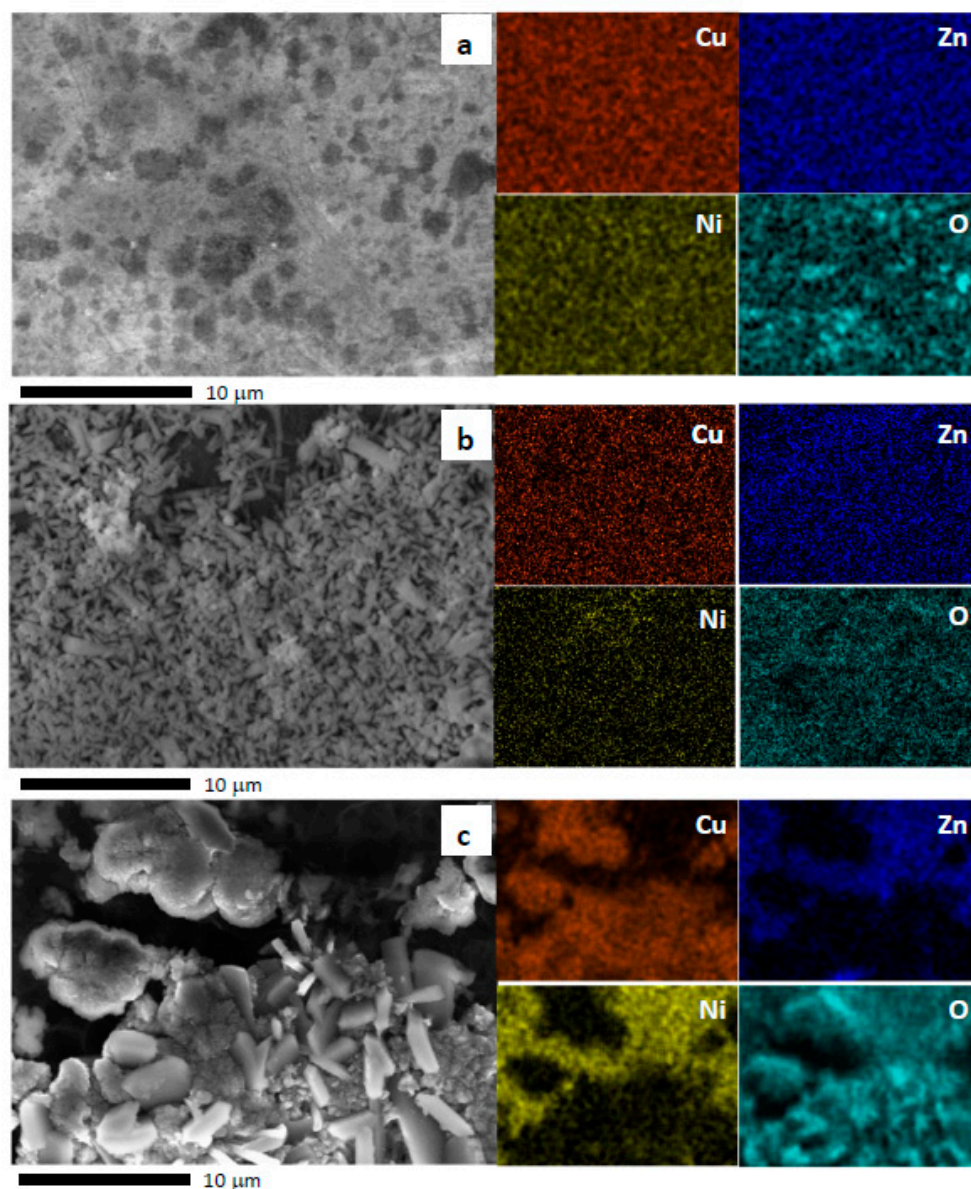


**Figure 3.** SEM-EDS analyses of samples obtained at 80 °C: (a) SEM of CuZnNi(1)80 sample (4000 X), (right) elemental mapping by EDS; (b) SEM of CuZnNi(2)80 sample, (right) elemental mapping; (c) SEM of CuZnNi(6)80 sample, (right) elemental mapping.

### 2.1.2. Growth of Nanooxides at Room Temperature

In view of the good qualities of the growths obtained, the possibility of their development at room temperature was analyzed. For this, the treatment was carried out at exposure times between 1 and 4 h, controlling the autoclave temperature at 25 °C and keeping all other conditions constant, such as the molar ratio of reagents and the arrangement of the substrates in the autoclave, among others. After these treatments, small mass increases in the samples were recorded since, as expected, the growth kinetics of the oxide crystals were much slower than those at 80 °C (Figure 1a). The effective development of crystalline oxide phases was confirmed, even for the sample with the shorter treatment time, as shown in Figure 4a. In the CuZnNi(1)RT sample, at bulk level, hydroxide and oxide phases of copper and zinc were observed as can be seen in the enlargement shown in Figure 4b. As the treatment time increased up to 6 h, the same phases coexisted although with a higher evolution of copper hydroxides/oxides, showing a picture similar to that previously discussed for treatments at higher temperatures, where the substrate surface was enriched

in copper species. Unlike the growths obtained at 80 °C, in this case, a bulk growth of NiO was not observed.

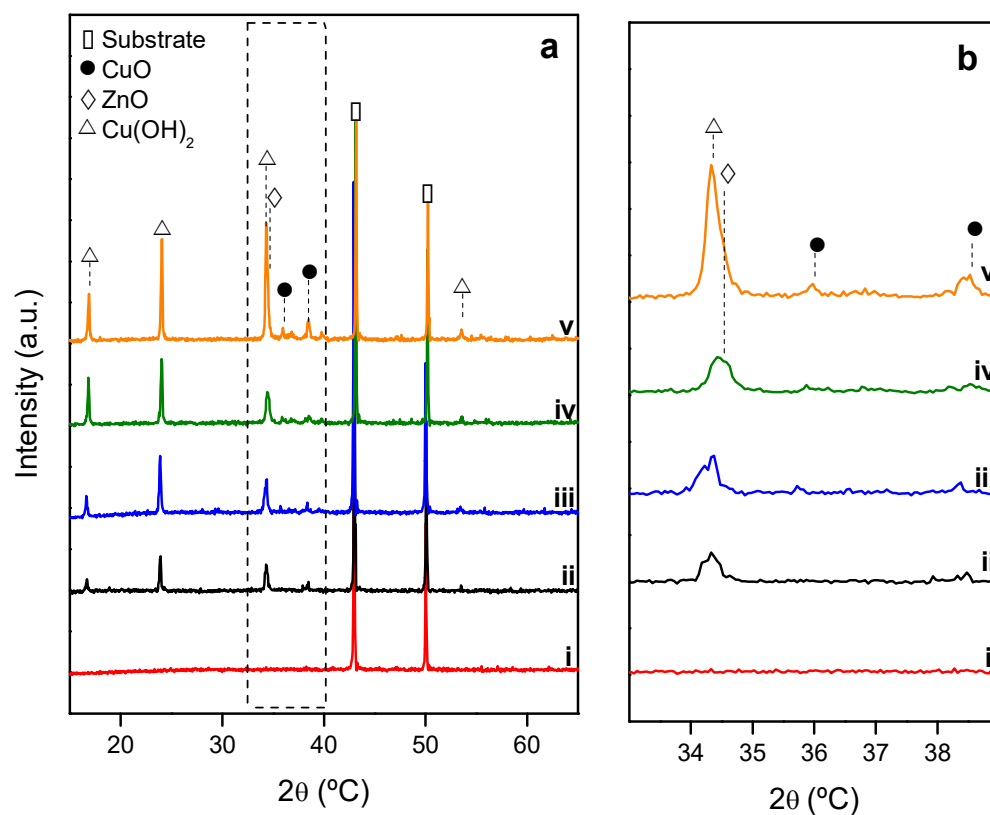


**Figure 4.** (a) XRD patterns of films grown on German silver substrates at room temperature (RT): (i) substrate; (ii) CuZnNi(1)RT; (iii) CuZnNi(2)RT; (iv) CuZnNi(4)RT; (v) CuZnNi(6)RT; (b) Detail of the diffractograms between  $2\theta$  33° and 39°.

The films synthesized at room temperature after one hour were obtained in a heterogeneous manner (Figure 5a), with some sectors rich in zinc and others in copper as shown by the elemental mapping of Figure 5b,c. The zinc-rich regions were made up of nanometric grains that densely covered the substrate (Figure 5d) and which, as observed in the image of Figure 5e, were formations with an interconnected dendritic-laminar shape, whereas in the copper-rich regions there developed sub-micrometric growths with cubic shape that densely covered these sectors (Figure 5f). A close view shows that they were polyhedral/cubic structures with an average size of about 300 nm (Figure 5g), which, according to what was determined by XRD and EDS, corresponds to copper oxides/hydroxides. After extending the treatment for 2 h, CuZnNi(2)RT, the surface still evolved in line with what was observed by XRD. The prismatic copper formations increased in size (Figure 5h), remaining above an underlying layer of laminar formations (inset Figure 5h) of Zn and Ni oxides, pointing a stratification process similar to that observed for higher temperatures. As shown in Figure 5i, copper oxides/hydroxides reached more defined facets and sizes between 0.5 and 1 micron, in line with a more developed crystalline growth. According to the elemental mappings for the CuZnNi(1)RT sample, the atomic relationships between the elements were similar to those obtained for the samples obtained at 80 °C, while for the CuZnNi(2)RT sample, said atomic relationships indicate a surface enrichment of Cu (Table 1), in total agreement with what was observed by XRD and SEM.

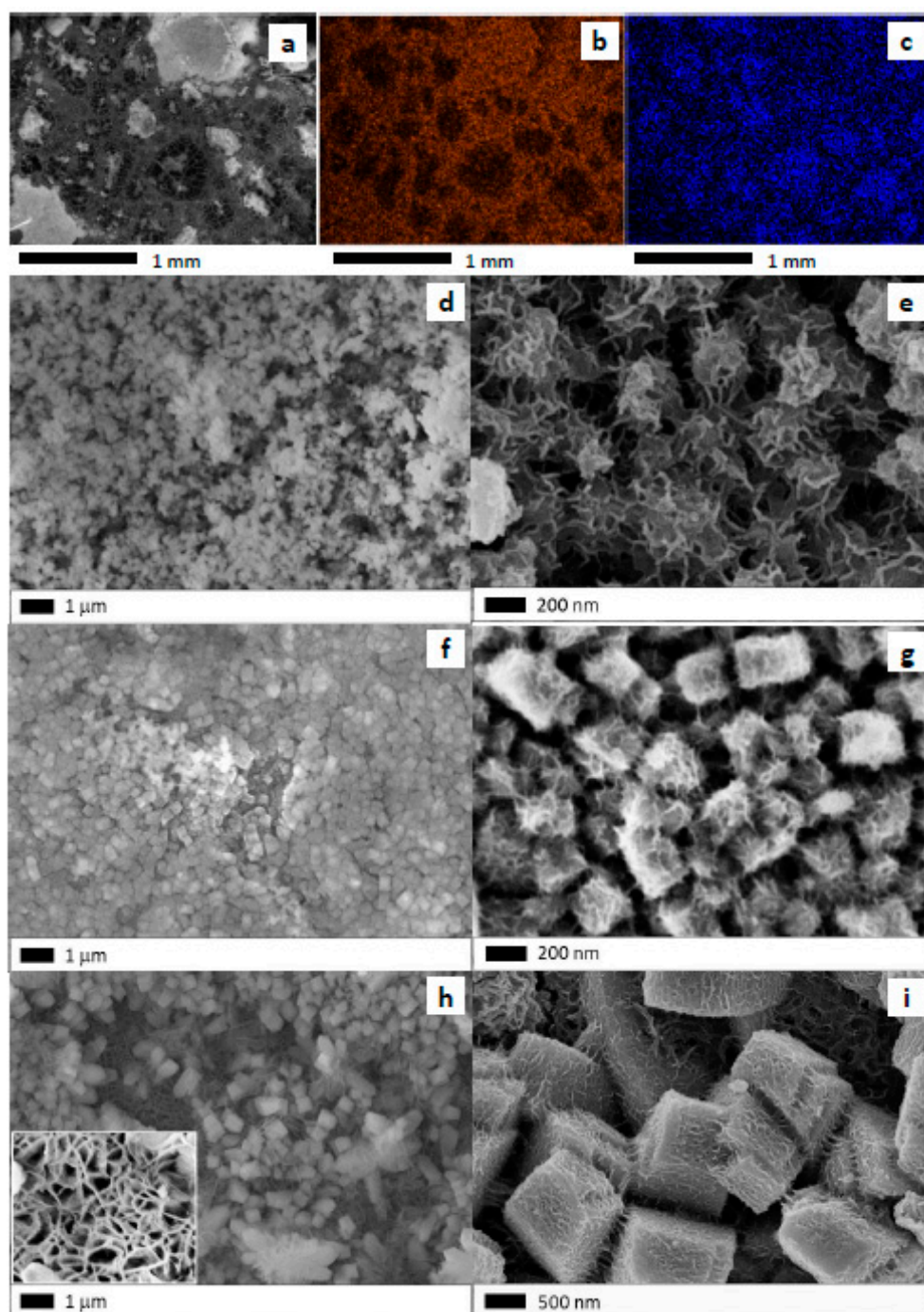


**Figure 5.** SEM-EDS images of samples synthesized at room temperature: (a) SEM view of the region analyzed by EDS in CuZnNi(1)RT; (b) elemental mapping of copper in CuZnNi(1)RT; (c) elemental mapping of zinc in CuZnNi(1)RT; (d) zinc-rich region of the CuZnNi(1)RT sample; (e) detail of the growth in zinc-rich region; (f) copper-rich region of the CuZnNi(1)RT sample; (g) detail of the growth in copper-rich region; (h) SEM of the CuZnNi(2)RT sample; (i) detail of the growth of (h).

It should be noted that the treatment temperature not only modified, as foreseeable, the kinetics of the growth of the oxides and, therefore, their size, but also their morphology as observed when comparing the SEM images of Figures 3 and 5. An interesting point to note is that under identical synthesis conditions, the growths of layered nano-oxides obtained from this alloy were different from those found in brass (Cu:Zn) [29]. In the present case, there remain nanometric and stable surface structures of copper hydroxides.

## 2.2. Catalytic Performance of CuZnNi Oxides Film

The results presented above show that it is possible to obtain firmly anchored growths of ternary nano-oxides from a common German-silver substrate, which are potentially interesting as catalysts for the CO oxidation reaction. In Figure 6a, the light-off curves obtained with the films synthesized at 80 °C are presented and it can be observed that all of them showed a remarkable catalytic behavior, reaching total conversion between 175 and 200 °C. The high activity of the nano-oxides is evident when compared with the profile of the untreated substrate (Figure 6a). The catalytic curves of the samples showed a similar and compressed profile in a narrow temperature range. However, the mass of oxides in each microreactor was very different (Table 2). Taking into account that the amount of oxygen incorporated during the oxidation treatment (mO) is relative to oxide mass, the ratio between the CO conversion at 150 °C ( $X_{150}$ ) and this mass of oxygen can be considered as a relative catalytic activity of the samples (Ra). This parameter clearly shows that the sample obtained after 1 h was the one with the highest relative activity (Table 2) and implies that the most superficial fraction of the nano-oxide layer acts efficiently in the reaction and that a higher increase in the layer thickness does not contribute new active sites. In other words, the conformation of the oxides in a thin film makes a high contact surface with the reactant stream, giving high efficiency. To analyze the stability of the films, the CuZnNi(1)80 sample was analyzed by XRD after the heat treatment in He carried out prior to the catalytic test. It can be noticed that the copper hydroxide phase decomposes into highly dispersed copper oxides (Figure S6). It is also notable that weak ZnO signals can hardly be perceived, with which these species also have enormously redispersed. Moreover, after subjecting this film to three consecutive cycles of catalytic runs, no changes in the XRD pattern were observed (Figure S6), signaling the stability in reaction of the nano-oxides.

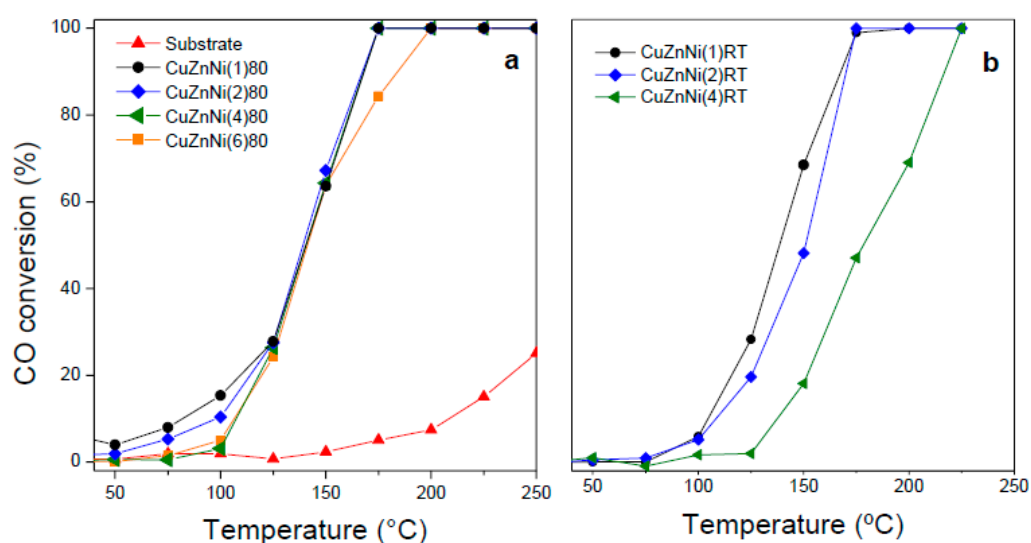


**Figure 6.** Catalytic behavior of nano-oxide-based microreactors in the CO oxidation reaction: (a) CuZnNi(x)80 samples; (b) CuZnNi(x)RT samples.

The activity of these films is ascribed to the presence of small phases of nano-oxides in close contact, which act synergically. Pioneering works of Taylor et al. [19] on CuO-ZnO catalysts obtained by coprecipitation showed the existence of a synergy when a solid solution is formed, which favors a strong electronic interaction between copper and zinc. However, this would not explain the case when the oxide phases are found separately. Recent studies have resumed the analysis of this aspect and confirmed a synergy between CuO-ZnO [34], which is attributed to electron transfer from ZnO to CuO, generating electron-rich heterojunctions, which are more favorable for the adsorption and dissociation of oxygen and the subsequent CO oxidation. Recently, the catalytic behavior of ZnO crystals with different morphologies onto which small CuO nanoparticles were dispersed

was analyzed. The modification of the fractions of different exposed facets of ZnO in contact with CuO led to different degrees of synergy, the (002) plane being the one that provided the greatest effect [11]. The formation of nanometer-sized CuO and ZnO phases in close contact on the surface of German silver allows a high number of interfaces that boost the activity in the CO oxidation reaction. This is also consistent with the catalytic behavior of growths obtained by the same method, but on copper substrates [16], which are made up exclusively of nanometric CuO<sub>x</sub>.

**Table 2.** Summary of the catalytic behavior of microreactors in the CO oxidation reaction.

Sample	mO <sup>a</sup>	T <sub>50</sub>	X <sub>150</sub> <sup>b</sup>	R <sub>a</sub> <sup>c</sup>
CuZnNi(1)80	5.9	142	63.6	10.8
CuZnNi(2)80	10.0	140	67.2	6.7
CuZnNi(4)80	13.7	142	64.3	4.7
CuZnNi(6)80	17.5	141	63.9	3.7
CuZnNi(1)RT	0.5	138	65.9	146.4
CuZnNi(2)RT	2.3	151	48.2	20.5
CuZnNi(4)RT	3.4	182	18.6	5.4

<sup>a</sup> Mass of oxygen incorporated by synthesis of the evaluated samples (mg), <sup>b</sup> CO conversion at 150 °C, <sup>c</sup> Relative activity: X<sub>150</sub>/mO.

Regarding the films synthesized at room temperature, it can be observed that they exhibited a notable performance that in some cases was even better than the ones obtained at a higher temperature (Figure 6b). Among the analyzed samples, CuZnNi(1)RT stands out since it showed the lowest T<sub>50</sub> (Table 2) in addition to the fact that the preparation of this catalyst implied a short treatment time (1 h) and without any energy consumption. The behavior of this catalytic film stands out if compared with that of similar films obtained by the same method onto copper [28] or brass substrates [29], showing the lowest T<sub>100</sub> and T<sub>50</sub> values as well as the highest Ra value. The high activity of this film is due to highly dispersed small nanometric CuO<sub>x</sub> and ZnO phases in close contact, which are also firmly stabilized onto the surface of the substrate, probably because they were generated through the direct growth from the substrate itself. Moreover, these films exhibited catalytic stability as observed in the consecutive runs performed applying ascending and descending temperature ramps (Figure 7a).

Given the outstanding behavior of the CuZnNi(1)RT film, it was subjected to a time-on reaction stability test bringing it to a temperature (~160 °C) that allowed its operation at conversions of 70–80% (Figure 7b). An initially slight deactivation was observed, which reduced the conversion level by 18% up to 12 h but then reached a stabilization, and the microreactor remained stable, giving the same level of conversion until the end of the 24 h test. This is a remarkable quality of this catalyst since it allowed an efficient and constant operation during a long reaction time under demanding conditions (conversions higher than 70%). This fact represents one of the main objectives when pursuing a development of a microreactor with an applied intention, in order to achieve the highest CO conversion at the lowest temperature and stability over time. Finally, it is proper to note that these oxide-based microreactors have extra potential given the surface topography of the catalytic film, which has intercrystalline nanometric interstices that make possible its subsequent modification with promoters such as ceria nanoparticles [35,36], which can further improve its performance in this reaction.

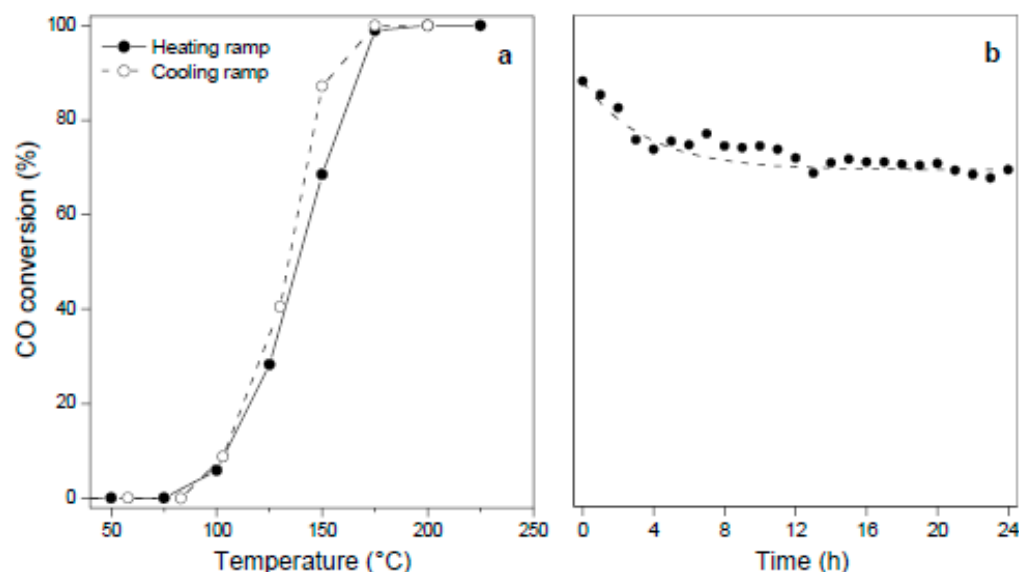


**Figure 7.** (a) Catalytic behavior of CuZnNi(1)RT sample after consecutive runs in heating and cooling ramps; (b) Catalytic stability under reaction during a 24 h assay.

### 3. Materials and Methods

#### 3.1. Synthesis of Nanostructured Oxide Films

Thin foils of German silver (100  $\mu\text{m}$  thickness) of common purity, cheap and easily available from non-ferrous metal suppliers, were used as substrates. First, they were washed with neutral soap and then in an ultrasonic bath with deionized water for 15 min and dried (80  $^{\circ}\text{C}$ , 10 min). Before synthesis, the foils were treated with a 5 wt. % HCl solution for 15 min, rinsed for 10 min with deionized water in an ultrasonic bath, and then put under the oxidation treatment. For the treatment, the substrates were placed vertically using a Teflon support in an autoclave above an equivolumetric mixture (10 mL) of  $\text{H}_2\text{O}_2$  (Cicarelli pro-analysis 100 vol) and  $\text{NH}_4\text{OH}$  (Anedra pro-analysis 28 wt. %). The treatments were carried out in a drying oven at 80  $^{\circ}\text{C}$  or at room temperature (25  $^{\circ}\text{C}$ ) for different times (1–16 h) after which the foils were washed with deionized water, dried (80  $^{\circ}\text{C}$ , 10 min), and finally weighed to determine the mass gain. The samples were denoted as CuZnNi(x)y, where x indicates the synthesis time in hours and y accounts for the treatment temperature ( $^{\circ}\text{C}$ ).

#### 3.2. Sample Characterization

The oxide formation was analyzed by X-ray diffraction (XRD) with an Empyrean PANalytical instrument ( $2^{\circ} \text{min}^{-1}$ ,  $\text{CuK}\alpha$ ,  $\lambda = 1.542 \text{ \AA}$ , 40 kV, 45 mA). The morphology and coverage of the oxides were studied by scanning electron microscopy (SEM) with an FE-SEM Zeiss Sigma instrument operated at 30 kV with a secondary electron detector InLens and a backscattering electron detector STEM module. The morphological detail in some samples was analyzed using the same instrument operated at 20 kV. Elemental microanalyses in small regions and elemental mappings were carried out by energy-dispersive X-ray spectroscopy (EDS) with a device coupled to the SEM instrument having a detector Oxford EDS with an area of 80  $\text{mm}^2$ . For the analyses, 20 keV of energy, 60  $\mu\text{m}$  aperture, and a Live Time of acquisition of 120 s were used. The working distance (WD) was 8.5 mm.

#### 3.3. Catalytic Performance in a Microreactor

Films grown on substrates with microchannels were tested in the CO oxidation through a microreactor module designed in our group, as indicated in previous work [37]. This was connected to a continuous flow system, equipped with mass flow controllers (Brooks 4800) and a PID temperature controller. Microreactors containing catalytic units with 117 microchannels, and with a mean hydraulic diameter of 300 microns, were evaluated.

Before evaluation, samples were pre-treated in He ( $30 \text{ mL min}^{-1}$ ) up to  $225 \text{ }^\circ\text{C}$  or  $250 \text{ }^\circ\text{C}$ , depending on the final temperature of the catalytic evaluation, respectively ( $5 \text{ }^\circ\text{C min}^{-1}$ ) and kept at this temperature for 30 min. Then, the catalytic reaction was carried out with a gaseous mixture of 1% CO and 2%  $\text{O}_2$  (molar composition) in He balance with a total flow of  $30 \text{ cm}^3 \text{ min}^{-1}$ . Measurements were made after stabilizing the samples for 10 min at different temperatures. CO conversion was obtained by analyzing the outlet gases with an on-line chromatograph (Shimadzu GC-2014) with a thermal conductivity detector (TCD) and a packed 5A zeolite column. CO to  $\text{CO}_2$  conversion was calculated as  $X = ([\text{CO}]^\circ - [\text{CO}])/[\text{CO}]^\circ$ ; where  $X$  is the conversion,  $[\text{CO}]^\circ$  and  $[\text{CO}]$  are the carbon monoxide concentrations before and after the reaction, respectively.

#### 4. Conclusions

Growths of  $\text{Cu}(\text{OH})_2$  and  $\text{CuO}$  nanostructures were obtained applying a simple oxidation treatment to German silver at  $80 \text{ }^\circ\text{C}$ , which changed the morphology with time from micrometric prismatic structures to globular-shaped oxide clusters. Meanwhile, as the treatment time elapsed, zinc and nickel oxides began to stratify above such copper species as nanosheets that grow from the substrate surface. These films showed a high catalytic performance in the CO oxidation reaction being active and reaching total conversion at  $175 \text{ }^\circ\text{C}$  with a  $T_{50}$  of  $142 \text{ }^\circ\text{C}$  and a stable catalytic response. When the vapor-based oxidation treatment was performed at room temperature, thin nanostructured films made of mixtures of copper oxide/hydroxide, zinc oxide, and nickel oxide highly dispersed on the substrate surface were produced. Among these synthesized films, the one obtained after one hour of treatment showed an outstanding catalytic behavior given the small and highly dispersed  $\text{CuO}_x$  and  $\text{ZnO}$  phases in close contact, which developed a synergy and were also firmly stabilized onto the substrate surface. Furthermore, they were quite stable under reaction conditions, keeping the nature of the active sites and reaching stable conversion levels under long reaction times. This novel microreactor was not only active and stable in the CO oxidation reaction but it came very close to the ideal concept of a green catalyst. This catalyst was made up of non-noble metal active phases placed onto a low-cost non-ferrous alloy support as a thin film, operating in a microreactor, and was obtained through a very simple and fast method (1 h) using a green oxidant, such as  $\text{H}_2\text{O}_2$ , and without energy consumption.

**Supplementary Materials:** The following supporting information can be downloaded at: <https://www.mdpi.com/article/10.3390/catal13060932/s1>. Figure S1. Photographs of samples obtained at  $80 \text{ }^\circ\text{C}$  after different synthesis time; Figure S2. SEM image and elemental mappings of bare German silver substrate: (a) SEM view of a region analyzed by EDS (magnification 1000 X); (b) elemental map of Cu; (c) elemental map of Zn; Figure S3. SEM image of the  $\text{CuZnNi}(2)80$  sample; Figure S4. SEM image and elemental mapping of the  $\text{CuZnNi}(2)80$  sample in another sector: (a) SEM view of the region analyzed by EDS (magnification 4000 X); (b) elemental map of Cu; (c) elemental map of O; (d) elemental map of Ni; (e) elemental map of Zn; Figure S5. SEM of the  $\text{CuZnNi}(6)80$  sample; Figure S6. XRD patterns of the  $\text{CuZnNi}(1)80$  sample: (a) fresh; (b) after pretreatment in He at  $200 \text{ }^\circ\text{C}$ ; (c) after successive catalytic runs.

**Author Contributions:** Conceptualization, J.M.Z.; Formal analysis, A.P.C. and M.A.F.M.; Funding acquisition, J.M.Z.; Investigation, A.P.C. and M.A.F.M.; Methodology, M.A.U. and J.M.Z.; Project administration, J.M.Z.; Resources, M.A.U. and J.M.Z.; Supervision, M.A.U. and J.M.Z.; Visualization, A.P.C., M.A.F.M., M.A.U. and J.M.Z.; Writing—original draft, A.P.C., M.A.F.M. and J.M.Z.; Writing—review & editing, A.P.C., M.A.U. and J.M.Z. All authors have read and agreed to the published version of the manuscript.

**Funding:** This research was funded by the Agencia Nacional de Promoción Científica y Tecnológica of Argentina (Project PICT 1880) and the Universidad Nacional del Litoral (Project CAI+D 00168LI). The authors also wish to thank the Consejo Nacional de Investigaciones Científicas y Técnicas (CONICET).

**Data Availability Statement:** The data presented in this study are available on request from the corresponding author.

**Conflicts of Interest:** The authors declare that they have no conflict of interest.

## References

1. Bullock, R.M. Reaction: Earth-Abundant Metal Catalysts for Energy Conversions. *Chem* **2017**, *2*, 444–446. [[CrossRef](#)]
2. Bion, N.; Can, F.; Courtois, X.; Duprez, D. Transition Metal Oxides for Combustion and Depollution Processes. In *Metal Oxides in Heterogeneous Catalysis*; Elsevier: Amsterdam, The Netherlands, 2018; pp. 287–353.
3. Chenoweth, J.A.; Albertson, T.E.; Greer, M.R. Carbon Monoxide Poisoning. *Crit. Care Clin.* **2021**, *37*, 657–672. [[CrossRef](#)] [[PubMed](#)]
4. Valdés-López, V.F.; Mason, T.; Shearing, P.R.; Brett, D.J.L. Carbon Monoxide Poisoning and Mitigation Strategies for Polymer Electrolyte Membrane Fuel Cells—A Review. *Prog. Energy Combust. Sci.* **2020**, *79*, 100842. [[CrossRef](#)]
5. Zamaro, J.M.; Boix, A.V.; Martínez-Hernández, A. CO Oxidation over Au Supported on Mn–ZSM5 and Mn–MOR. *Catal. Commun.* **2015**, *69*, 212–216. [[CrossRef](#)]
6. Abedi, A.; Luo, J.Y.; Epling, W.S. Improved CO, Hydrocarbon and NO Oxidation Performance Using Zone-Coated Pt-Based Catalysts. *Catal. Today* **2013**, *207*, 220–226. [[CrossRef](#)]
7. Zhou, Y.; Wang, Z.; Liu, C. Perspective on CO Oxidation over Pd-Based Catalysts. *Catal. Sci. Technol.* **2015**, *5*, 69–81. [[CrossRef](#)]
8. Camposeco, R.; Maturano-Rojas, V.; Zanella, R. Highly Efficient Au/ZnO–ZrO<sub>2</sub> Catalysts for CO Oxidation at Low Temperature. *Catalysts* **2023**, *13*, 590. [[CrossRef](#)]
9. Saoud, K.M.; El-Shall, M.S. Physical and Chemical Synthesis of Au/CeO<sub>2</sub> Nanoparticle Catalysts for Room Temperature CO Oxidation: A Comparative Study. *Catalysts* **2020**, *10*, 1351. [[CrossRef](#)]
10. Duan, D.; Hao, C.; He, G.; Wang, H.; Shi, W.; Gao, L.; Sun, Z. Co<sub>3</sub>O<sub>4</sub> Nanosheet/Au Nanoparticle/CeO<sub>2</sub> Nanorod Composites as Catalysts for CO Oxidation at Room Temperature. *ACS Appl. Nano Mater.* **2020**, *3*, 12416–12426. [[CrossRef](#)]
11. Lu, S.; Song, H.; Xiao, Y.; Qadir, K.; Li, Y.; Li, Y.; He, G. Promoted Catalytic Activity of CO Oxidation at Low Temperatures by Tuning ZnO Morphology for Optimized CuO/ZnO Catalysts. *Colloid Interface Sci. Commun.* **2023**, *52*, 100698. [[CrossRef](#)]
12. Du, L.; Wang, W.; Yan, H.; Wang, X.; Jin, Z.; Song, Q.; Si, R.; Jia, C. Copper-Ceria Sheets Catalysts: Effect of Copper Species on Catalytic Activity in CO Oxidation Reaction. *J. Rare Earths* **2017**, *35*, 1186–1196. [[CrossRef](#)]
13. Zhang, H.; Zhang, Y.; Song, H.; Cui, Y.; Xue, Y.; Wu, C.; Pan, C.; Xu, J.; Qiu, J.; Xu, L. Transition Metal (Fe<sub>2</sub>O<sub>3</sub>, Co<sub>3</sub>O<sub>4</sub> and NiO)-Promoted CuO-Based  $\alpha$ -MnO<sub>2</sub> Nanowire Catalysts for Low-Temperature CO Oxidation. *Catalysts* **2023**, *13*, 588. [[CrossRef](#)]
14. Hu, X.; Mao, D.; Yu, J.; Xue, Z. Low-Temperature CO Oxidation on CuO–CeO<sub>2</sub>–ZrO<sub>2</sub> Catalysts Prepared by a Facile Surfactant-Assisted Grinding Method. *Fuel* **2023**, *340*, 127529. [[CrossRef](#)]
15. Stoian, M.; Maurer, T.; Lamri, S.; Fehete, I. Techniques of Preparation of Thin Films: Catalytic Combustion. *Catalysts* **2021**, *11*, 1530. [[CrossRef](#)]
16. Wiame, F.; Maurice, V.; Marcus, P. Initial Stages of Oxidation of Cu<sub>0.7</sub>Zn<sub>0.3</sub>(1 1 1). *Surf. Sci.* **2007**, *601*, 4402–4406. [[CrossRef](#)]
17. Lee, S.; Kim, S.; Kim, T.; Lin, C.; Lee, W.-J.; Kim, S.-J.; Gorte, R.J.; Jung, W. The Effects of Iron Oxide Overlayers on Pt for CO Oxidation. *Catal. Commun.* **2022**, *172*, 106549. [[CrossRef](#)]
18. Xu, L.; Pan, Y.; Li, H.; Xu, R.; Sun, Z. Highly Active and Water-Resistant Lanthanum-Doped Platinum-Cobalt Oxide Catalysts for CO Oxidation. *Appl. Catal. B Environ.* **2023**, *331*, 122678. [[CrossRef](#)]
19. Taylor, S.H.; Hutchings, G.J.; Mirzaei, A.A. The Preparation and Activity of Copper Zinc Oxide Catalysts for Ambient Temperature Carbon Monoxide Oxidation. *Catal. Today* **2003**, *84*, 113–119. [[CrossRef](#)]
20. Wang, D.; Xu, R.; Wang, X.; Li, Y. NiO Nanorings and Their Unexpected Catalytic Property for CO Oxidation. *Nanotechnology* **2006**, *17*, 979–983. [[CrossRef](#)]
21. Jeong, M.-G.; Kim, I.H.; Han, S.W.; Kim, D.H.; Kim, Y.D. Room Temperature CO Oxidation Catalyzed by NiO Particles on Mesoporous SiO<sub>2</sub> Prepared via Atomic Layer Deposition: Influence of Pre-Annealing Temperature on Catalytic Activity. *J. Mol. Catal. A Chem.* **2016**, *414*, 87–93. [[CrossRef](#)]
22. Chen, Z.; Xie, Y.L.; Qiu, J.X.; Chen, Z.H. Characterization and Catalytic Activity of CuO and NiO Supported on ZrO<sub>2</sub> for CO Low Temperature Oxidation. *Adv. Mater. Res.* **2013**, *842*, 237–241. [[CrossRef](#)]
23. El-Shobaky, G.A.; Yehia, N.S.; Hassan, H.M.A.; Badawy, A.R.A.A. Catalytic Oxidation of CO by O<sub>2</sub> over Nanosized CuO–ZnO System Prepared under Various Conditions. *Can. J. Chem. Eng.* **2009**, *87*, 792–800. [[CrossRef](#)]
24. Soliman, N.K. Factors Affecting CO Oxidation Reaction over Nanosized Materials: A Review. *J. Mater. Res. Technol.* **2019**, *8*, 2395–2407. [[CrossRef](#)]
25. Zamaro, J.M.; Miró, E.E. Copper Alloy Microstructures for Application in Microreactors. In *Copper Alloys: Preparation, Properties and Applications*; Nova Science Publishers Inc.: New York, NY, USA, 2011; pp. 127–139.
26. Groppi, G.; Airoidi, G.; Cristiani, C.; Tronconi, E. Characteristics of Metallic Structured Catalysts with High Thermal Conductivity. *Catal. Today* **2000**, *60*, 57–62. [[CrossRef](#)]
27. Neyertz, C.A.; Gallo, A.D.; Ulla, M.A.; Zamaro, J.M. Nanostructured CuO<sub>x</sub> Coatings onto Cu Foils: Surface Growth by the Combination of Gas-Phase Treatments. *Surf. Coat. Technol.* **2016**, *285*, 262–269. [[CrossRef](#)]
28. Papurello, R.L.; Cabello, A.P.; Ulla, M.A.; Neyertz, C.A.; Zamaro, J.M. Microreactor with Copper Oxide Nanostructured Films for Catalytic Gas Phase Oxidations. *Surf. Coat. Technol.* **2017**, *328*, 231–239. [[CrossRef](#)]
29. Cabello, A.P.; Ulla, M.A.; Zamaro, J.M. In Situ Growth of Nanostructured Copper and Zinc Mixed Oxides on Brass Supports as Efficient Microreactors for the Catalytic CO Oxidation. *J. Mater. Sci.* **2022**, *57*, 12797–12809. [[CrossRef](#)]

30. Neikov, O.D.; Naboychenko, S.S.; Murashova, I.B. Production of Copper and Copper Alloy Powders. In *Handbook of Non-Ferrous Metal Powders*; Elsevier: Amsterdam, The Netherlands, 2019; pp. 571–614.
31. Amin, A.; El-dissouky, A. One-Step Synthesis of Novel  $\text{Cu}_2\text{ZnNiO}_3$  Complex Oxide Nanowires with Tuned Band Gap for Photoelectrochemical Water Splitting. *J. Appl. Crystallogr.* **2020**, *53*, 1425–1433. [[CrossRef](#)]
32. Bahnasawy, N.; Elbanna, A.M.; Ramadan, M.; Allam, N.K. Fabrication of Polyhedral Cu–Zn Oxide Nanoparticles by Dealloying and Anodic Oxidation of German Silver Alloy for Photoelectrochemical Water Splitting. *Sci. Rep.* **2022**, *12*, 16785. [[CrossRef](#)]
33. Babikier, M.; Wang, D.; Wang, J.; Li, Q.; Sun, J.; Yan, Y.; Yu, Q.; Jiao, S. Cu-Doped ZnO Nanorod Arrays: The Effects of Copper Precursor and Concentration. *Nanoscale Res. Lett.* **2014**, *9*, 199. [[CrossRef](#)]
34. Lyu, S.; Zhang, Y.; Li, Z.; Liu, X.; Tian, Z.; Liu, C.; Li, J.; Wang, L. Electronic Metal-Support Interactions Between  $\text{Cu}_x\text{O}$  and ZnO for  $\text{Cu}_x\text{O}/\text{ZnO}$  Catalysts with Enhanced CO Oxidation Activity. *Front. Chem.* **2022**, *10*, 912550. [[CrossRef](#)] [[PubMed](#)]
35. Cabello, A.P.; Ulla, M.A.; Zamaro, J.M.  $\text{CeO}_2/\text{CuO}_x$  Nanostructured Films for CO Oxidation and CO Oxidation in Hydrogen-Rich Streams Using a Micro-Structured Reactor. *Top. Catal.* **2019**, *62*, 931–940. [[CrossRef](#)]
36. Pérez, N.C.; Miró, E.E.; Zamaro, J.M. Microreactors Based on  $\text{CuO}-\text{CeO}_2/\text{Zeolite}$  Films Synthesized onto Brass Microgrids for the Oxidation of CO. *Appl. Catal. B Environ.* **2013**, *129*, 416–425. [[CrossRef](#)]
37. Papurello, R.L.; Fernández, J.L.; Miró, E.E.; Zamaro, J.M. Microreactor with Silver-Loaded Metal-Organic Framework Films for Gas-Phase Reactions. *Chem. Eng. J.* **2017**, *313*, 1468–1476. [[CrossRef](#)]

**Disclaimer/Publisher’s Note:** The statements, opinions and data contained in all publications are solely those of the individual author(s) and contributor(s) and not of MDPI and/or the editor(s). MDPI and/or the editor(s) disclaim responsibility for any injury to people or property resulting from any ideas, methods, instructions or products referred to in the content.